

## Design, Synthesis, and Preliminary Evaluation of Doxazolidine Carbamates as Prodrugs Activated by Carboxylesterases

David J. Burkhart,<sup>†,‡</sup> Benjamin L. Barthel,<sup>†,‡</sup> Glen C. Post,<sup>†</sup> Brian T. Kalet,<sup>†</sup> Jordan W. Nafie,<sup>†</sup> Richard K. Shoemaker,<sup>†</sup> and Tad H. Koch<sup>\*,†,§</sup>

Department of Chemistry and Biochemistry, University of Colorado, Boulder, Colorado 80309-0215, and University of Colorado Cancer Center, Aurora, Colorado 80010

Received May 18, 2006

The synthesis and tumor cell growth inhibition by doxazolidine carbamate prodrugs are reported. The carbamates were designed for selective hydrolysis by one or more human carboxylesterases to release doxazolidine (Doxaz), the formaldehyde–oxazolidine of doxorubicin that cross-links DNA to trigger cell death. Simple butyl and pentyl, but not ethyl, carbamate prodrugs inhibited the growth of cancer cells that overexpress carboxylesterase CES1 (hCE1) and CES2 (hiCE). Relative CES1 and CES2 expression levels were determined by reverse transcription of the respective mRNAs, followed by polymerase chain reaction amplification. More complex structures with a *p*-aminobenzyl alcohol (PABA) self-eliminating spacer showed better growth inhibition (IC<sub>50</sub> = 50 nM for Hep G2 liver cancer cells) while exhibiting reduced toxicity toward rat cardiomyocytes, relative to the parent drug doxorubicin. Pentyl 4-(*N*-doxazolidinylcarbonyloxymethyl)phenylcarbamate, the lead compound for further investigation, appears to be activated in Hep G2 cells that express both CES1 and CES2.

### Introduction

Doxazolidine (Doxaz<sup>a</sup>) is the oxazolidine derivative resulting from the reaction of the antitumor drug doxorubicin (Dox) at its vicinal aminol functional group with formaldehyde (Chart 1). Further reaction with formaldehyde couples two Doxaz molecules at their oxazolidine nitrogens via a methylene group to yield doxoform (Doxf, Chart 1).<sup>1,2</sup> Circumstantial evidence now implicates Doxaz as the active metabolite of Dox that virtually cross-links DNA, leading to tumor cell death.<sup>2,3</sup> Doxf is a very labile prodrug of Doxaz. Doxf and, correspondingly, Doxaz are 10- to 10 000-fold more active than Dox for growth inhibition of sensitive and resistant cancer cells. Measurements of the kinetics of spontaneous hydrolysis of Doxf to Doxaz to Dox indicate that the half-lives of Doxf and Doxaz with respect to hydrolysis to Dox under physiological conditions are approximately 1–3 min.<sup>2</sup> Starting with Doxf, the slower of the two steps is the hydrolysis of Doxaz to Dox. In spite of its short half-life, Doxaz is taken up rapidly by cancer cells and exhibits excellent cytotoxicity. For in vivo treatment of tumors, release of Doxaz from a hydrolytically robust prodrug by an enzyme overexpressed at the site of the tumor should increase tumor response and minimize side effects, especially treatment-limiting cardiotoxicity associated with doxorubicin therapy.<sup>4</sup> Although oxazolidine rings are known to hydrolyze rapidly in aqueous media, their *N*-carbamate derivatives are quite stable (Chart 1). The design of such a hydrolytically stable derivative is suggested by the structures of two new clinical prodrugs, capecitabine and irinotecan.

\* To whom correspondence should be addressed. Phone: 303-492-6193. Fax: 303-492-5894. E-mail: tad.koch@colorado.edu.

<sup>†</sup> University of Colorado.

<sup>‡</sup> These authors contributed equally to this work.

<sup>§</sup> Colorado Cancer Center.

<sup>a</sup> Abbreviations: Butyl PABC-Doxaz, butyl 4-(*N*-doxazolidinylcarbonyloxymethyl)phenyl-carbamate; CES, carboxylesterase; Dox, doxorubicin; Doxaz, doxazolidine, the formaldehyde oxazolidine derivative of doxorubicin; Doxf, doxoform, *N,N'*-bis-doxazolidinylmethane; 5-FU, 5-fluorouracil; PABA, *p*-aminobenzyl alcohol; PABC, *p*-aminobenzylloxycarbonyl; pentyl PABC-Doxaz, pentyl 4-(*N*-doxazolidinylcarbonyloxymethyl)phenylcarbamate; RT-PCR, reverse transcriptase–polymerase chain reaction.

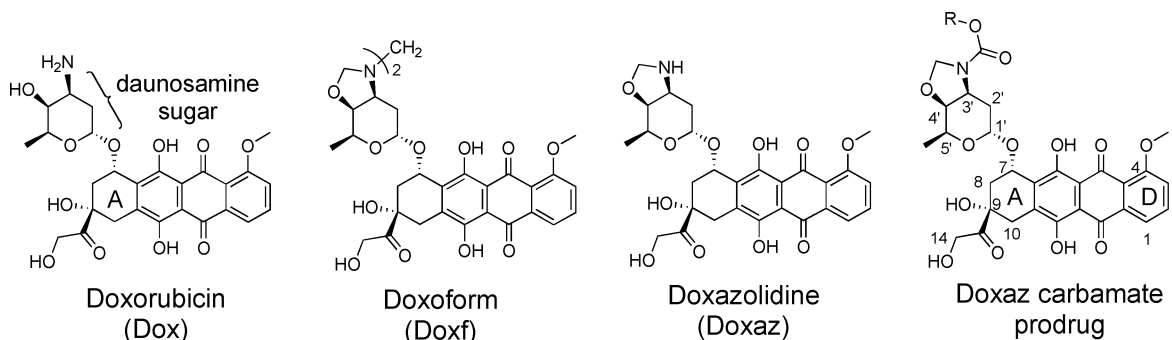
Capecitabine is the pentyl carbamate of a 5-fluorocytidine derivative that functions as a prodrug of the antitumor compound 5-fluorouracil (5-FU).<sup>5,6</sup> In vivo activation requires three enzymatic steps, the first of which is hydrolysis of the pentyl carbamate functional group by a carboxylesterase (Scheme 1). Capecitabine is a substrate for human carboxylesterases CES1 (hCE1) and CES2 (hiCE), with CES1 being the more active enzyme.<sup>7</sup> CES1 is a promiscuous serine hydrolase, overexpressed in numerous types of cancer cells and malignant tissue, and it appears in both cytosolic and microsomal fractions.<sup>8,9</sup> Irinotecan is a carbamate prodrug of a water soluble camptothecin and is hydrolyzed primarily in colon and primary colon tumors by CES2, also a serine hydrolase.<sup>10,11</sup> In spite of the substantial structural differences between capecitabine and irinotecan, they are both hydrolyzed by carboxylesterases CES1 and CES2, but in general CES1 prefers a smaller alcohol moiety as in capecitabine and CES2, a larger alcohol moiety as in irinotecan. Carboxylesterases also play a significant role in the metabolism and elimination of numerous xenobiotics, including cocaine and heroin.<sup>12</sup> The substrate selectivity of carboxylesterases stems from a pair of recognition pockets. One pocket is a small, rigid cavity that commonly recognizes small alcohol or ester functional groups and the other is a large flexible pocket capable of accommodating numerous substrates for hydrolysis.<sup>13,14</sup>

We began our search for a hydrolytically robust Doxaz prodrug by synthesizing simple carbamates analogous to the carbamate in capecitabine. Doxaz has a cytotoxic selectivity for cancer cells, and this prodrug strategy has the potential for additional selectivity because prodrug activation requires the overexpression of a carboxylesterase. In addition, a small lipophilic carbamate moiety could increase the rate of prodrug uptake without completely sacrificing water solubility.

### Results and Discussion

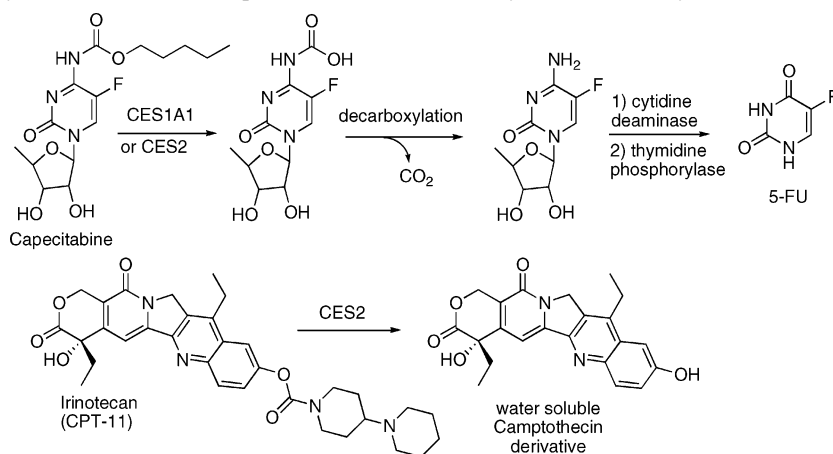
**Synthesis and Characterization of Simple Doxazolidine Carbamates.** The synthesis of simple Doxaz carbamates was achieved by addition of the modestly nucleophilic Doxaz to the

**Chart 1** Clinical Drug Doxorubicin, Potent Cytotoxins Doxoform and Doxazolidine (Doxaz), and Proposed Carbamate Prodrug of Doxazolidine Rendering the Oxazolidine Ring Hydrolytically Stable<sup>a</sup>

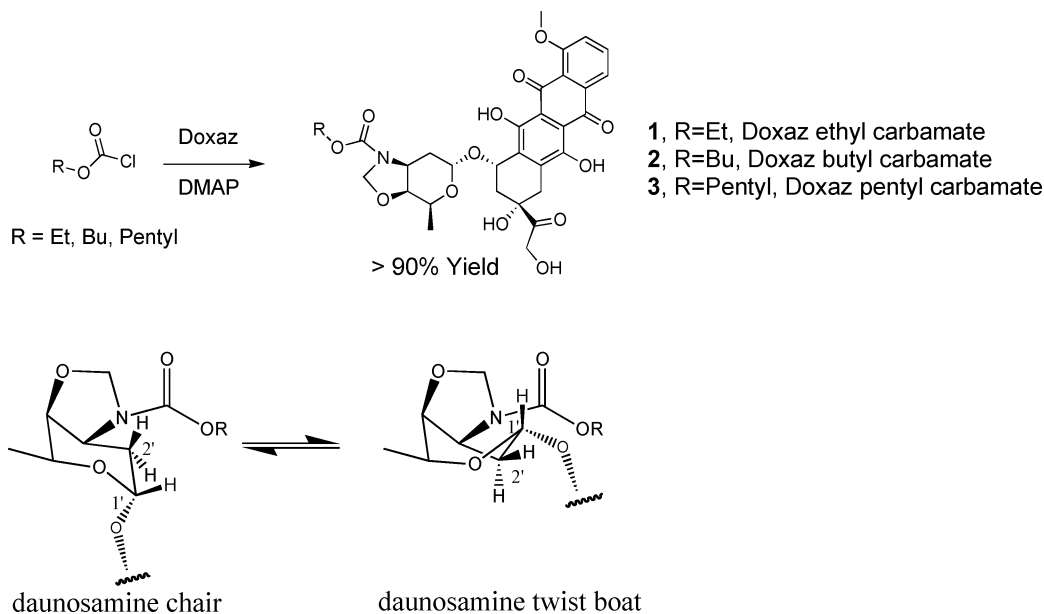


<sup>a</sup> The numbering scheme adopted is that traditionally used for the anthracyclines.

**Scheme 1.** Proposed Enzymatic Activation of Capecitabine and Irinotecan by Human Carboxylesterases



**Scheme 2.** Synthesis of Hydrolytically Robust Doxaz Carbamates **1**, **2**, and **3** and Proposed Chair–Twist-Boat Conformational Equilibrium of the Daunosamine Amino Sugar Ring Showing the Change in Dihedral Angles between the Hydrogens at the 1'- and 2'-Positions



desired alkyl chloroformate buffered by 1.1 equiv of dimethylaminopyridine (DMAP) or to the desired alkyl *p*-nitrophenyl carbonate. The crude Doxaz carbamates were purified directly by radial chromatography and obtained in good yield (compounds **1**, **2**, and **3**; Scheme 2). The structures were established from one and two-dimensional <sup>1</sup>H NMR spectra and mass spectral molecular ions. Two-dimensional homonuclear NMR

experimental data facilitated the assignment of proton NMR resonances. Resonances in the ambient temperature <sup>1</sup>H NMR spectra showed line broadening, indicating conformational exchange at a rate similar to the NMR time scale.

Variable temperature NMR experiments with the ethyl carbamate (**1**) confirmed the presence of conformational dynamics. Exchange rate constants determined at multiple temperatures

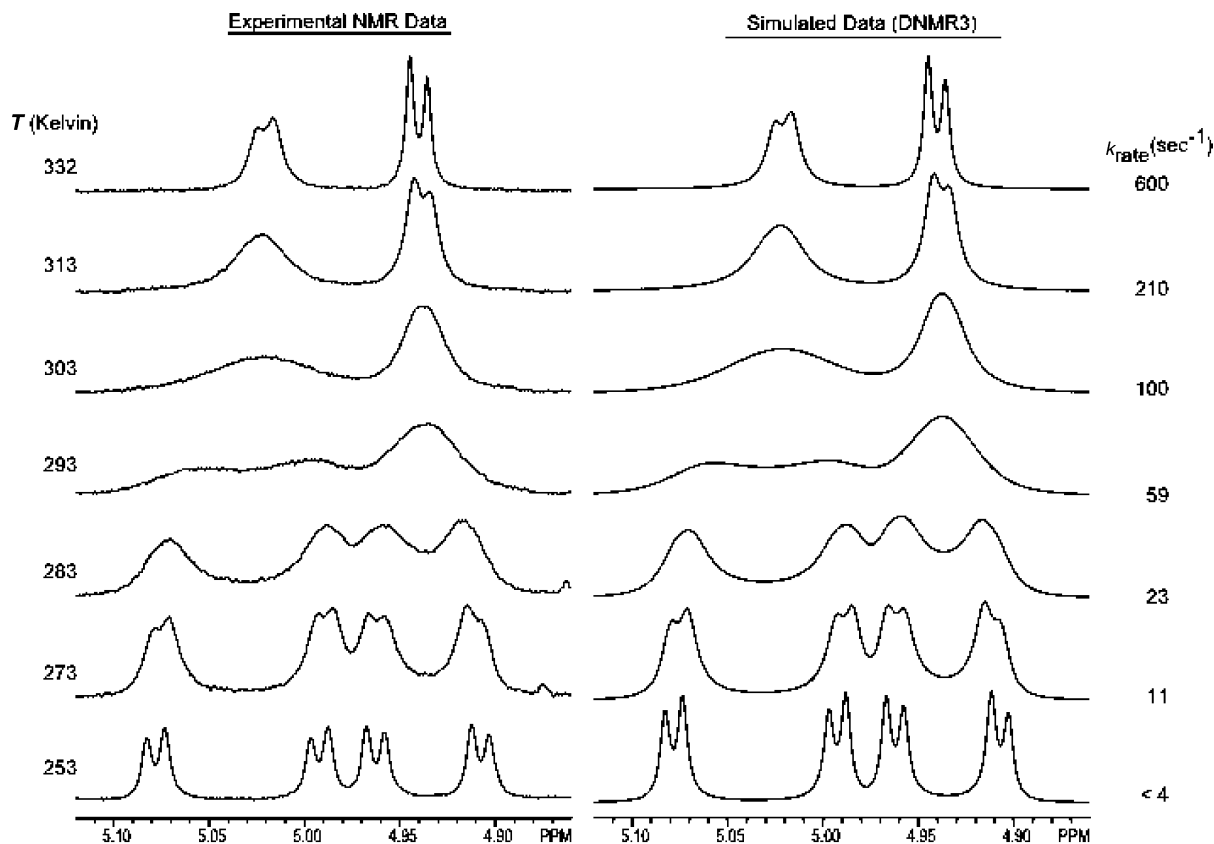


**Figure 1.** Variable-temperature  $^1\text{H}$  NMR of Doxaz ethyl carbamate (**1**) to resolve the oxazolidine methylene (4.9–5.1 ppm) resonances and determine the energy of interconversion between conformations.

(via spectral simulation) revealed the thermodynamic parameters,  $\Delta H^\ddagger$ ,  $\Delta S^\ddagger$ , and  $\Delta G^\ddagger$ , associated with the barrier between the two conformers. Experimental and simulated NMR spectra of the oxazolidine methylene resonances at all temperatures are shown in Figure 1. At the low-temperature limit, the oxazolidine methylene protons appear as two AB patterns that collapse into one AB pattern at the high-temperature limit. Integration of the AB patterns at the low-temperature limit establishes that the conformational populations are approximately equal. To achieve quality dynamic simulations, the AB patterns were first simulated under static conditions (using the NUMARIT algorithm), after which dynamic simulations (DNMR3) were performed using the previously simulated peak frequencies. The free energy barrier ( $\Delta G^\ddagger$ ) for the interconversion between the conformations as determined from the dynamic NMR results is  $61.8 \pm 1.6$  kJ/mol at 293 K. Analysis of the slope and Y-intercept of an Eyring plot yields  $\Delta H^\ddagger = 49.0 \pm 1.3$  kJ/mol and  $\Delta S^\ddagger = -45 \pm 5$  J/mol $^{-1}\text{K}^{-1}$ .

One possible explanation for the conformational exchange is bond rotation about the C–N bond of the carbamate functional group. Although not required by symmetry, the conformational populations might be approximately equal as observed. However, careful earlier measurements on simpler carbamates report a  $\Delta H^\ddagger$  in deuteriochloroform of  $75 \pm 0.5$  kJ/mol and a  $\Delta S^\ddagger$  of only  $1 \pm 1$  J/mol $^{-1}\text{K}^{-1}$  for this rotational barrier.<sup>15</sup> The  $\Delta S^\ddagger$  observed for the conformational dynamics of Doxaz ethyl carbamate is clearly inconsistent with a simple carbamate bond rotation. Further, the conformational change appears to be complex, involving the oxazolidine ring and the daunosamine sugar, as well as the tetracycline A-ring, because proton resonances in all three rings show coalescence as the temperature is increased. Additional proton resonances that show more dramatic temperature dependence of chemical shift include one

of the protons at the 2'-position and one of the protons at the 10-position (see Chart 1 for the numbering scheme). A possible conformational change in the daunosamine sugar is a chair to twist-boat interconversion, as shown with energy-minimized molecular models in Figure 2. This conformational change would have a much larger effect on the chemical shift of one of the protons at the 2'-position than the other (see Scheme 1). The dihedral angle defined by the 1'-C–O bond to the anomeric oxygen and one of the 2'-C–H bonds changes from approximately  $180^\circ$  to  $60^\circ$  in going from twist-boat to chair. The corresponding dihedral angle relating the other proton at the 2'-position is approximately  $60^\circ$  in both conformations. The NMR spectra at the lowest temperature did not show sufficient resolution for determination of the respective coupling constants. The entropy of activation for this chair–twist boat interconversion is likely to be large because molecular models suggest that the transition state will be relatively rigid. For the chair–twist boat interconversion of cyclohexane itself,  $\Delta H^\ddagger = 42.5 \pm 0.4$  kJ/mol and  $\Delta S^\ddagger = -11.71 \pm 2.1$  J/mol $^{-1}\text{K}^{-1}$ .<sup>16</sup> Also consistent with the proposal is the recent observation of a twist-boat conformation for the daunosamine sugars in the crystal structure of Doxf.<sup>2</sup> The NMR spectra, however, of both Doxf and Doxaz in chloroform solvent at ambient temperature are consistent with a predominant chair conformation for their respective daunosamine sugars, with no conformational exchange at a rate similar to the NMR time scale.<sup>2</sup> The difference between the energy of chair and the energy of twist-boat conformations of Doxaz versus Doxaz carbamates likely results from the difference in the hybridization of their respective oxazolidine nitrogens,  $\text{sp}^3$  versus  $\text{sp}^2$ . A twist-boat conformation should alleviate some of the oxazolidine ring strain associated with an  $\text{sp}^2$  nitrogen in a five-member ring fused to a six-member ring. The reduction in ring strain is needed to

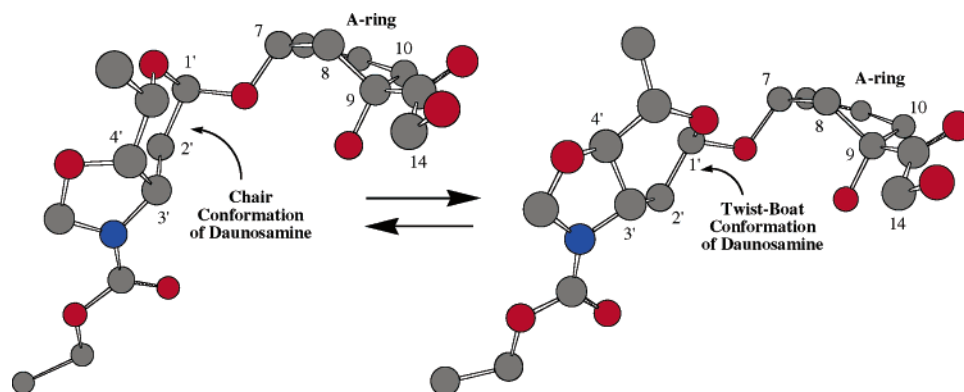


**Figure 2.** Molecular models showing the proposed chair and twist-boat conformations of the daunosamine sugar of Doxaz ethyl carbamate (**1**). Framework structures of the A-ring, daunosamine, and oxazolidine with daunosamine in chair and twist-boat conformations were created in ChemDraw and energy minimized in Chem3D. The numbering system is the anthracycline numbering system shown in Chart 1.

balance the increased torsional strain and loss of some of the anomeric effect associated with a twist-boat conformation.

#### Biological Activity of Simple Doxazolidine Carbamates.

Because the prodrug carbamates were designed to be activated by CES1 and/or CES2, cell lines of interest were measured for expression of the respective mRNAs using reverse transcription (RT), followed by PCR (polymerase chain reaction). Cancer cell lines investigated included SHP-77 resistant small cell lung, DU-145 prostate, MCF-7 sensitive breast, MCF-7/Adr resistant breast, SK-HEP-1 liver, and Hep G2 liver cells. As a measure of possible cardiotoxicity, H9c2(2-1) rat cardiomyocytes were also investigated. Cardiotoxicity is relevant because the ultimate product of metabolism and subsequent hydrolysis of these carbamates is doxorubicin, which is cardiotoxic.<sup>4</sup> Primers corresponding to the 5', middle, and 3' regions of human or rat CES1 and CES2 were identified by Primer Express (Applied Biosystems, Foster City, CA). Each primer set produced a single, compact band by agarose gel electrophoresis at the predicted size, indicating that PCR with the primer sequences amplified only those regions that were targeted. Sequences for all primers are provided in Supporting Information. The results of the RT-PCR (Figure 3) show that both liver cancer cell lines, SK-HEP-1 and Hep G2, strongly express the mRNA for CES2, however, only the Hep G2 cell line strongly expresses the mRNA for CES1. DU-145, MCF-7, and MCF-7/Adr cells express more CES2 than CES1, and SHP-77 cells express both enzymes, but in lesser amounts than Hep G2 cells. Additionally, the rat cardiomyocytes, H9c2(2-1), also express more CES2 than CES1.

Cell growth inhibition experiments initially focused on MCF-7, MCF-7/Adr, SK-HEP-1, and Hep G2 cancer cells, as well as rat cardiomyocytes, as a measure of cardiotoxicity and Vero cells (green monkey kidney cells) as an additional measure of normal cell toxicity. The butyl and pentyl carbamates inhibited the growth of MCF-7, MCF-7/Adr, and SK-HEP-1 cell lines with a 24 h drug treatment period, with some selectivity for cancer cells over cardiomyocytes relative to growth inhibition by Dox, as shown in Table 1. The ethyl carbamate with the least complex structure exhibited poor cancer cell growth inhibition. The relative inactivity of the ethyl carbamate may indicate that a substantial lipophilic interaction is required at the active site of the carboxylesterases to hold the Doxaz substrate. For all measurements with the pentyl carbamate, the IC<sub>50</sub> values were dependent on drug treatment time. With a 3 h drug treatment period, the log IC<sub>50</sub> values for MCF-7, SK-HEP-1, and Hep G2 cells were greater than -6 compared to -6.5 to -7 for identical treatments with doxorubicin. This is consistent with only a small fraction of the butyl **2** and pentyl **3** carbamates

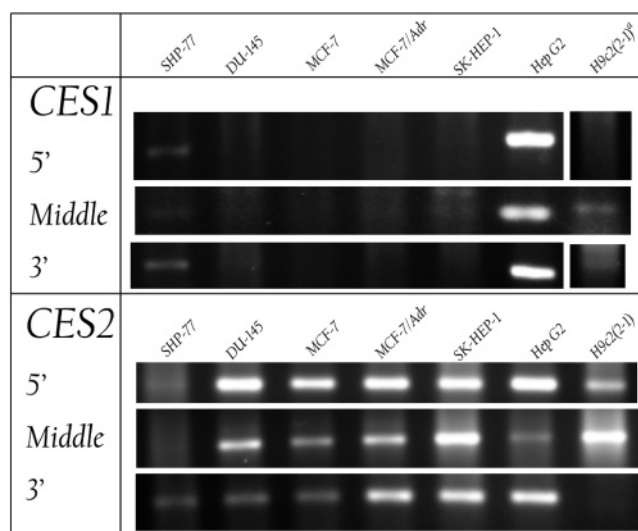


**Figure 3.** Relative expression of mRNAs for carboxylesterases CES1 and CES2 by SHP-77 small cell lung, DU-145 prostate, MCF-7 sensitive breast, MCF-7/Adr resistant breast, SK-HEP-1 liver, and Hep G2 liver cancer cells, and rat cardiomyocytes (H9c2(2-1)). mRNAs were reverse transcribed, and DNA was amplified by the PCR using three different primers specific for the 5', middle, and 3' regions of the genes. The DNA was separated by agarose gel electrophoresis and detected with ethidium bromide staining. (a) The vertical bars indicate nonadjacent gel lanes.

being hydrolyzed during the 24 h drug treatment because the log IC<sub>50</sub> for Doxaz with SK-HEP-1 cells is -8.4 and with Hep G2, -8.0, and over many cancer cell lines, -8.5 to -8.0, all with 3 h drug treatment (a few of these are reported in Table 1). A control experiment showed that the pentyl carbamate is stable to hydrolysis in pH 7.4 buffer in the absence of cells or growth media over 24 h at ambient temperature, monitoring the reaction by HPLC.

Uptake of the pentyl carbamate **3** relative to uptake of Dox was measured by flow cytometry, monitoring fluorescence of the Dox fluorophore as a measure of the drug in cells. The measurements were performed over a period of 3 h in the presence and absence of fetal bovine serum, and the results are shown in Figure 4. Clearly, the pentyl carbamate was taken up at a higher level and more rapidly than Dox. Further, the presence of 10% fetal bovine serum decreased the uptake of doxorubicin and the pentyl carbamate by about 25%. The more rapid uptake of the pentyl carbamate in the presence and absence of serum probably reflects its increased hydrophobicity relative to that of doxorubicin, which is a cation at physiological pH.

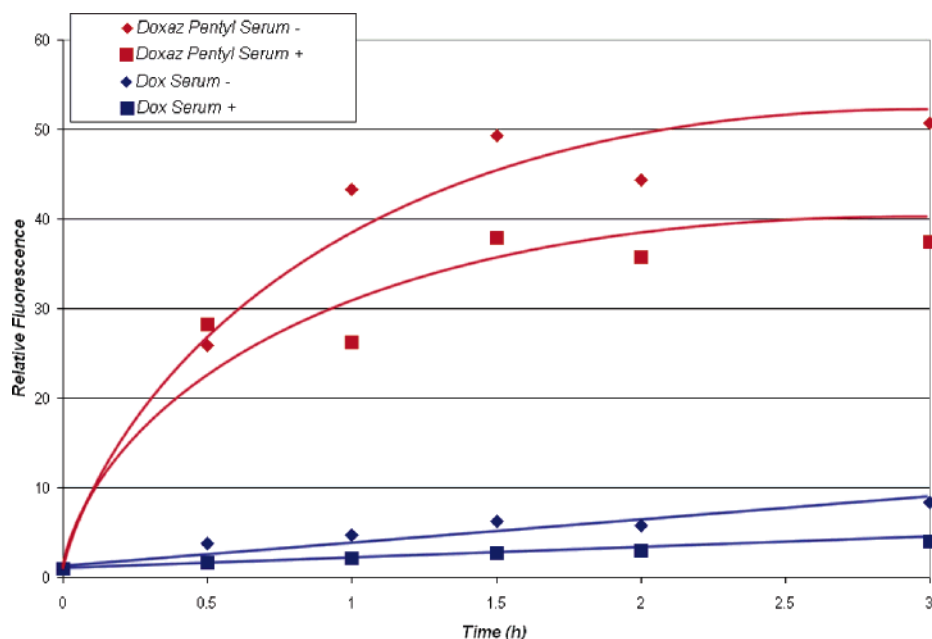


**Figure 4.** Uptake of Dox or the Doxaz pentyl carbamate (**3**) by SK-HEP-1 liver cancer cells, as determined by flow cytometry, measuring relative fluorescence of the Dox fluorophore as a function of treatment time in RPMI media containing 10% fetal bovine serum (+) and RPMI media with no serum (–). Drug concentration in media was 0.5  $\mu$ M.

**Table 1.** Growth Inhibition and IC<sub>50</sub> Values<sup>a</sup>

drug/cell line, treatment time	1		2		3	
	Dox	Doxaz ethyl carbamate	Doxaz butyl carbamate	Doxaz pentyl carbamate	Doxaz	
MCF-7, 3 h	–6.5 <sup>b</sup>	> –6		> –6	–8.5 ± 0.03 <sup>c</sup>	
24 h	–7.9 ± 0.04	> –6	–6.1 ± 0.04	–6.1 ± 0.03	–8.5 ± 0.03 <sup>c</sup>	
MCF-7/Adr, 3 h	–5.2 ± 0.1	–5.3 ± 0.04			–8.4 ± 0.1	
24 h	–5.6 ± 0.1	> –5	–6.2 ± 0.3	–6.0 ± 0.09	–8.0 ± 0.08	
SK-HEP-1, 3 h	–7.0 ± 0.1	> –6		> –6	–8.2 ± 0.04	
24 h	–7.3 ± 0.2	> –6	–6.4 ± 0.2	–6.7 ± 0.1	–8.1 ± 0.3	
Hep G2, 3 h	–6.7 ± 0.09	> –6		> –6	–8.1 ± 0.3	
24 h	–7.5 ± 0.1	> –6	–6.7 ± 0.3	–6.5 ± 0.3	–8.1 ± 0.3	
H9c2(2-1), 3 h	–7.5 ± 0.2	–5.8 ± 0.2			–8.1 ± 0.3	
24 h	–7.7 ± 0.3		–5.8 ± 0.2	–6.6 ± 0.1	–8.1 ± 0.3	
Vero, 3 h	–6.0 ± 0.02			–5.4 ± 0.1	–8.1 ± 0.3	
24 h	–6.3 ± 0.08		–6.3 ± 0.1	–5.3 ± 0.01	–8.1 ± 0.3	

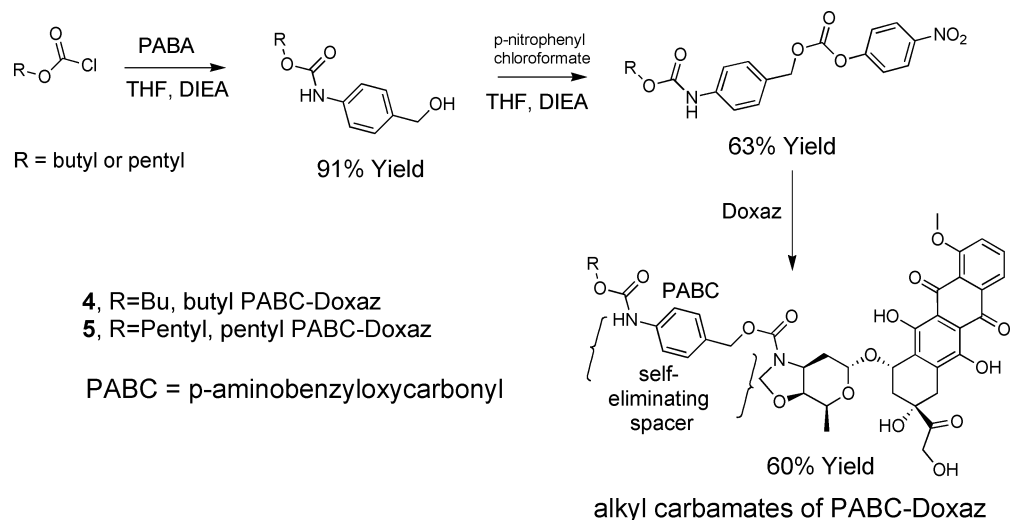
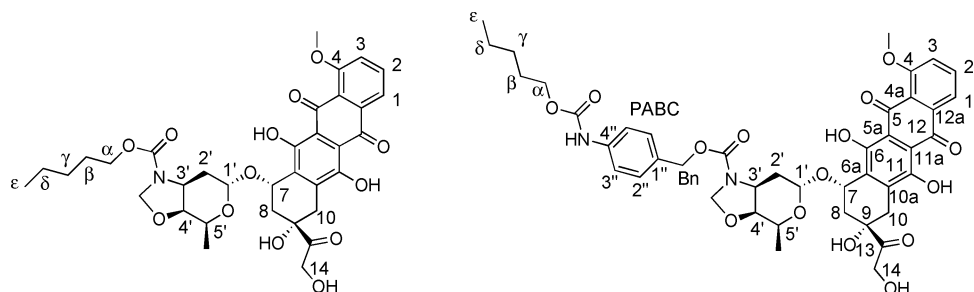
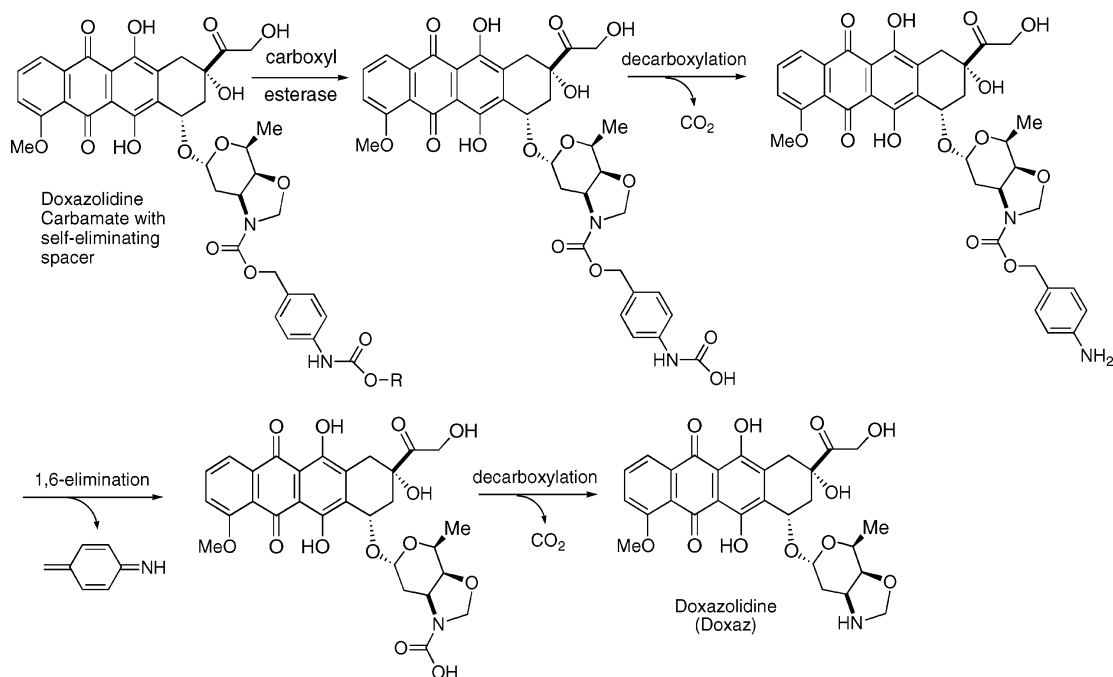
<sup>a</sup> IC<sub>50</sub> values are reported as the log of the molar concentration of sensitive breast (MCF-7), resistant breast (MCF-7/Adr), and liver (SK-HEP-1 and Hep G2) cancer cells, as well as noncancerous rat cardiomyocytes (H9c2(2-1)) and green monkey kidney cells (Vero) with 3 and/or 24 h drug treatments with Doxaz alkyl carbamates (**1**, **2**, and **3**) versus treatment with Dox or Doxaz. Viability of cells was assayed with crystal violet, except viability of H9c2(2-1) cells treated for 3 h and of Vero cells treated for 3 or 24 h, which were assayed with MTT. <sup>b</sup> Reference 1. <sup>c</sup> Reference 2.

Increased hydrophobicity may also be the explanation for the effect of serum on the uptake of the carbamate; namely, the carbamate binds to serum proteins, reducing drug uptake.

**Synthesis and Characterization of Doxazolidine Carbamates with Self-Eliminating Spacer.** The growth inhibition data in Table 1 together with our experience and that of others with prodrugs suggested drug efficacy might be improved by adding a self-eliminating spacer between the alkyl carbamate functionality and the anthracycline.<sup>17–19</sup> This could present the lipophilic carbamate to the enzyme with significantly less steric bulk and increase the rate of enzymatic hydrolysis. A Katzenellenbogen-type spacer from *p*-aminobenzyl alcohol (PABA) often works well in this capacity.<sup>20</sup> The spacer was incorporated by reacting PABA with the desired chloroformate, followed by conversion to the *p*-nitrophenyl carbonate ester and reaction with Doxaz, as shown in Scheme 3. The structures again were established from NMR spectra and mass spectral molecular ions. The <sup>1</sup>H NMR spectra at ambient and elevated temperatures also showed evidence of conformational dynamics. Spectra of the pentyl PABC-Doxaz, pentyl 4-(*N*-doxazolidinylcarbonyloxymethyl)-phenylcarbamate (**5**), at ambient and elevated temperature, are

supplied in the Supporting Information, and chemical shift assignments for all the protons and carbons at 55 °C are reported in the Experimental Section, with the numbering scheme given in Chart 2. Proton and carbon chemical shifts were established from the combination of high-resolution 1D proton, homonuclear COSY, HSQC, and HMBC spectra. Activation of these carbamates is predicted to occur by enzymatic hydrolysis of the alkyl carbamate, followed by rapid decarboxylation at the anilino carbamic acid and 1,6-elimination of imino quinone methide, as shown in Scheme 4. A second spontaneous decarboxylation step releases Doxaz.

**Biological Activity of Doxazolidine Carbamates with Self-Eliminating Spacer.** Growth inhibition experiments with butyl and pentyl carbamates bearing the PABA self-eliminating spacer (compounds **4** and **5**) focused on Hep G2 liver cancer cells that strongly express both CES1 and CES2 and SK HEP-1 cells that express significantly more CES2 than CES1. SHP-77 small cell lung cancer cells were also of interest because they express modest amounts of both enzymes. Inhibition of the growth of cardiomyocytes was used as a measure of cardiotoxicity, and inhibition of the growth of Vero cells, green monkey kidney

**Scheme 3.** Synthesis of Doxaz Carbamates **4** and **5** with Self-Eliminating PABC Spacer**Chart 2.** Numbering Scheme for Doxaz Alkyl Carbamates and Alkyl PABC-Doxaz Derivatives for the Assignment of Proton and Carbon Chemical Shifts in the Experimental Section**Scheme 4.** Proposed Enzymatic Activation of Alkyl PABC-Doxaz Prodrugs (**4** and **5**)

cells, was again used as another measure of toxicity to normal cells. Clearly, both the butyl and the pentyl carbamates with PABA spacer are more active than the simple carbamates, as shown in Table 2. They also show more activity against the cancer cells that express higher levels of CES1. Of particular note is the higher activity against Hep G2 cells than against SK-HEP-1 cells. This suggests that CES1 is more active than

CES2. Pentyl PABC-Doxaz (**5**) also shows more than 1 order of magnitude lower toxicity to cardiomyocytes and Vero cells than to Hep G2 and SHP-77 cells. The low toxicity of pentyl PABC-Doxaz to cardiomyocytes relative to the toxicity of Dox is encouraging and consistent with the low level of expression of CES1 in cardiomyocytes, as shown in Figure 3.

Uptake of pentyl PABC-Doxaz (**5**) and Dox by multidrug

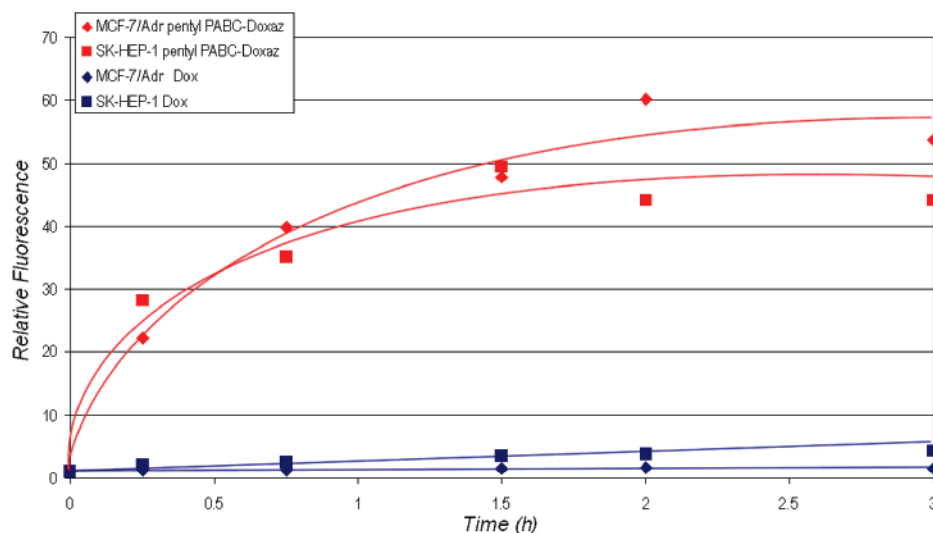


**Figure 5.** Uptake of Dox or pentyl PABC-Doxaz (**5**) by MCF-7/Adr breast and SK-HEP-1 liver cancer cells, as determined by flow cytometry, measuring relative fluorescence of the Dox fluorophore as a function of treatment time in RPMI media containing 10% fetal bovine serum. Drug concentration in media was 0.5  $\mu$ M.

**Table 2.** Cell Growth Inhibition Values ( $IC_{50}$ ) Expressed in Log of Molar Concentrations for Doxaz Alkyl Carbamates (**2** and **3**) and Alkyl PABC-Doxaz Compounds (**4** and **5**) Compared with Dox for 24 h Drug Treatment<sup>a</sup>

drug/cell line	Dox	<b>2</b> Doxaz butyl carbamate	<b>4</b> butyl PABC-Doxaz	<b>3</b> Doxaz pentyl carbamate	<b>5</b> pentyl PABC-Doxaz
MCF-7	-7.9 $\pm$ 0.04	-6.1 $\pm$ 0.04	-4.1 $\pm$ 0.3	-6.1 $\pm$ 0.03	-5.6 $\pm$ 0.3
MCF-7/Adr	-5.6 $\pm$ 0.1	-6.2 $\pm$ 0.3	-5.9 $\pm$ 0.06	-6.0 $\pm$ 0.09	-6.5 $\pm$ 0.06
DU-145	-7.5 $\pm$ 0.08	-6.4 $\pm$ 0.02	-6.3 $\pm$ 0.3	-6.0 $\pm$ 0.04	-6.7 $\pm$ 0.07
SHP-77	-6.9 $\pm$ 0.05	-6.6 $\pm$ 0.3	-7.1 $\pm$ 0.1	-6.3 $\pm$ 0.3	-7.3 $\pm$ 0.1
HepG2	-7.5 $\pm$ 0.1	-6.7 $\pm$ 0.3	-7.7 $\pm$ 0.03	-6.5 $\pm$ 0.3	-7.3 $\pm$ 0.2
SK-HEP-1	-7.3 $\pm$ 0.2	-6.4 $\pm$ 0.2	-5.8 $\pm$ 0.04	-6.7 $\pm$ 0.1	-6.0 $\pm$ 0.06
H9c2(2-1)	-7.7 $\pm$ 0.3	-5.8 $\pm$ 0.2	-7.2 $\pm$ 0.2	-6.6 $\pm$ 0.1	-6.2 $\pm$ 0.2
Vero	-6.3 $\pm$ 0.08	-6.3 $\pm$ 0.1	-6.1 $\pm$ 0.08	-5.3 $\pm$ 0.01	-6.0 $\pm$ 0.04

<sup>a</sup> Cancer cells are defined in the legends to Table 1 and Figure 3. Growth inhibition of cardiomyocytes (H9c2(2-1)) is a measure of cardiotoxicity, and growth inhibition of Vero cells (green monkey kidney cells) is a second measure of toxicity to normal cells. Viability of cells was assayed with crystal violet, except the viability of Vero cells which were assayed with MTT.

resistant MCF-7/Adr breast cancer cells and SK-HEP-1 liver cancer cells in the presence of fetal bovine serum is compared in Figure 5, as determined by flow cytometry using drug fluorescence as a measure of the drug in cells. Pentyl PABC-Doxaz is taken up much better by both cell lines than Dox. Better uptake probably results from increased hydrophobicity and the absence of positive charge; Dox is a cation at physiological pH, whereas the pentyl PABC-Doxaz is uncharged. Release of pentyl PABC-Doxaz and Dox from MCF-7/Adr and SK-HEP-1 cells was also measured by flow cytometry, measuring drug fluorescence as a function of time after 3 h drug treatment, as shown in Figure 6. The Dox fluorophore is released from both cell lines treated with pentyl PABC-Doxaz at approximately an equal rate, with apparent faster and then slower first-order kinetics. The half-lives are 0.3 and 30 h, respectively. Disappearance of the Dox fluorophore from Dox-treated cells is faster and appears to follow simple first-order kinetics from MCF-7/Adr cells with a half-life of approximately 0.1 h. With Dox-treated SK-HEP-1 cells, the initial release is similar but appears to plateau after the faster release, as observed with pentyl PABC-Doxaz-treated cells, but at an order of magnitude lower level. MCF-7/Adr cells are known to over-express P-170 glycoprotein efflux pump. Substrates for this efflux pump commonly bear hydrophobic regions as well as a positive charge, characteristic of Dox but not of pentyl PABC-Doxaz.<sup>21</sup> So, we conclude that pentyl PABC-Doxaz is taken up better and retained better than Dox in SK-HEP-1 liver cancer

cells and the MDR expressing MCF-7/Adr cancer cells, mostly because of its increased hydrophobicity.

The cell growth inhibition data together with the mRNA expression data implicate CES1 as the primary enzyme responsible for activation of Doxaz carbamates, and this activation likely occurs inside cells where the enzyme resides. Further evidence comes from measurement of the lack of hydrolysis of the prodrug in phosphate-buffered saline (PBS) or phosphate-buffered fetal bovine serum (FBS). HPLC analysis of the hydrolysis reactions after 24 h at 37 °C showed an intact drug, no formation of doxorubicin, and no formation of the product from loss of formaldehyde from the carbamate, namely, the pentyl carbamate of PABC-Dox. The fraction of carbamates hydrolyzed in Hep G2 liver cancer cells is still estimated to be low (in the range of 10% over 24 h), because the  $IC_{50}$  values are high relative to the values for Doxaz. Similar inefficiency is observed for carboxylesterase hydrolysis of capecitabine and irinotecan, and inefficient hydrolysis is a desirable property for a carboxylesterase-activated prodrug to minimize side effects.<sup>22</sup>

The hydrolysis experiment required a higher concentration of the pentyl PABC-Doxaz (**5**), 50  $\mu$ M, than the cell experiments because of the sensitivity of the HPLC analytical method. This higher concentration necessitated a method of formulation, because pentyl PABC-Doxaz is not soluble in PBS or FBS at 50  $\mu$ M concentration. Several excipients were explored, including various cyclodextrins, cremophor ELP, Tween 80, and bovine albumin in combination with DMSO. Cremophor ELP/

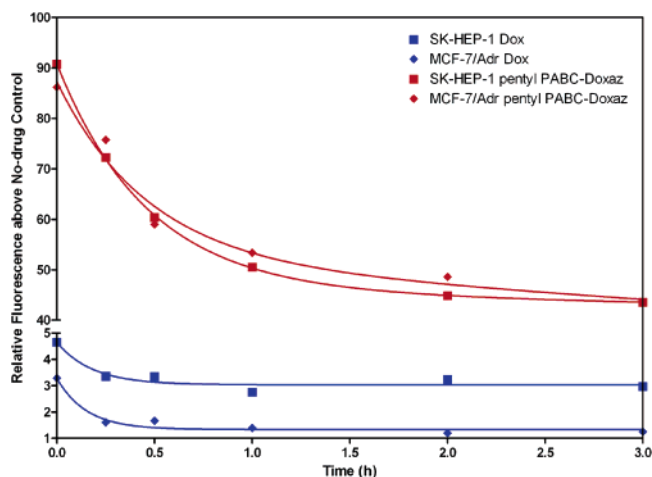


**Figure 6.** Release of Dox or pentyl PABC-Doxaz (**5**) by MCF-7/Adr breast and SK-HEP-1 liver cancer cells, as determined by flow cytometry, measuring relative fluorescence of the Dox fluorophore as a function of time after  $0.5 \mu\text{M}$  drug treatment for 3 h in RPMI media containing 10% fetal bovine serum. The y-scale was expanded at low fluorescence to allow presentation of data for both drugs in the same graph. Release of pentyl PABC-Doxaz was fit with a double exponential rate law, giving half-lives of  $3 \times 10^{-1}$  h and  $3 \times 10^1$  h for both cell lines with  $R^2 = 0.9998$  with SK-HEP-1 cells and  $0.9769$  with MCF-7/Adr cells. Insufficient signal was obtained for similar analysis of Dox release, but the half-life for the faster release was approximately  $1 \times 10^{-1}$  h.

DMSO, polysorbate 80 (Tween 80)/DMSO, and bovine albumin/DMSO emerged as successful candidates. Pentyl PABC-Doxaz is completely soluble at  $50 \mu\text{M}$  when a  $100\times$  solution in 1:1 DMSO/cremaphor ELP (v/v) or 1:1 DMSO/Tween 80 (v/v) is diluted 100-fold with either PBS or FBS. Bovine albumin/DMSO was also successful, except a small fraction of the red color from the drug appeared at the bottom of the Eppendorf tube upon centrifugation of the solution at  $16\,600 \times g$ . Any of these formulations should be suitable for future *iv* exploratory animal experiments. Cremophor ELP is used in the formulation of paclitaxel, and Tween 80 is used in the formulation of docetaxel, but not without some side effects with each excipient.<sup>23</sup>

As a further predictor of survival of the pentyl PABC-Doxaz in the vascular system, prodrug concentration was measured after 24 h at  $37^\circ\text{C}$  in pooled human plasma. Pentyl PABC-Doxaz was quantitated in three separate experiments at times 0 and 24 h by HPLC, detecting prodrug both by absorption at 480 nm and by fluorescence at 550 nm. The average survival of prodrug over all six measurements was  $82 \pm 8\%$ .

## Conclusions

The very active but hydrolytically unstable derivative of doxorubicin, doxazolidine, is stabilized to hydrolysis by carbamylation of its oxazolidine nitrogen. The ethyl carbamate is inactive, and the butyl and pentyl carbamates show modest inhibition of the growth of some cancer cell lines. RT-PCR measurements suggest both carboxylesterase CES1 and CES2 as possible activating enzymes. More favorable cancer cell growth inhibition was achieved by including a PABA self-eliminating spacer in the design to separate the alkyl carbamate functional group from the bulky anthracycline. The lead compound, pentyl PABC-Doxaz (**5**), shows similar growth inhibition of Hep G2 primary liver cancer cells and better growth inhibition of SHP-77 small cell lung cancer cells than doxorubicin. Further, pentyl PABC-Doxaz shows better drug uptake and retention and much lower growth inhibition of cardiomyo-

cytes and Vero cells than doxorubicin. In fact, doxorubicin is more toxic to cardiomyocytes than to Hep G2 cells, but **5** is at least 10-fold more toxic to Hep G2 cells than to cardiomyocytes. These properties together with the favorable drug uptake and retention by the MDR expressing MCF-7/Adr cells and stability in plasma indicate that **5** should be explored further using *in vivo* models of liver cancer or other cancers whose cells overexpress CES1 and CES2 or possibly other carboxylesterase enzymes. Primary liver cancer, or hepatocellular carcinoma (HCC), is diagnosed in over 14 000 patients per year and leads to approximately 9500 deaths in the United States each year.<sup>24</sup> Despite its low incidence in western society, HCC is almost invariably fatal, and it is the third highest cancer-related cause of death in men and the seventh in women worldwide.<sup>25–27</sup> Further, its incidence in the U.S. is predicted to accelerate in the next two to three decades.<sup>28</sup>

## Experimental Section

**1. General Remarks.** Doxorubicin hydrochloride clinical samples (formulated with lactose) were received as a gift from FeRx (Aurora, CO). Pharmaceutical grade Tween 80 was a gift from Tapestry Pharmaceuticals, Inc., Boulder, CO. Doxazolidine was synthesized as previously described.<sup>2</sup> DMSO and chloroform were prepared by addition of activated  $4 \text{ \AA}$  molecular sieves for at least 48 h prior to use. Dichloromethane was distilled from calcium hydride prior to use. NMR solvents were purchased from Cambridge Isotope Laboratories, Inc (Andover, MA). All other chemicals were purchased from Aldrich (Milwaukee, WI) and used without further purification. Analytical HPLC was performed on a Hewlett-Packard/Agilent 1050/1100 chromatograph equipped with auto injector, diode array UV-vis absorption detector, and fluorescence detector interfaced to an Agilent ChemStation data system (Palo Alto, CA). Analytical HPLC injections were onto an Agilent Zorbax  $5 \mu\text{m}$  reverse-phase octadecylsilyl (ODS) column,  $4.6 \text{ mm i.d.} \times 150 \text{ mm}$ , eluting at  $1.0 \text{ mL/min}$  with method 1, a gradient of acetonitrile/20 mM triethylammonium acetate buffer, pH 7.4 (80% buffer to 70% buffer at 5 min to 30% buffer at 15 min, then isocratic to 25 min) or with method 2, a gradient of acetonitrile/20 mM triethylammonium acetate buffer, pH 7.6 (60% buffer to 0% buffer at 10 min, isocratic until 12 min, and to 60% buffer at 15 min. The eluent was monitored for absorption at 280 and 480 nm and/or for fluorescence at 550 nm with excitation at 480 nm. All NMR spectra were performed using Varian Unity INOVA 400 and 500 MHz spectrometers (Palo Alto, CA). All spin simulations and dynamic NMR simulations were performed using SpinWorks 2.4 software by Kirk Marat (SpinWorks software is available at [ftp://davincci.chem.umanitoba.ca/pub/marat/SpinWorks](http://davincci.chem.umanitoba.ca/pub/marat/SpinWorks)). Sample temperatures for the dynamic NMR experiments were calibrated using the separation between hydroxyl resonance and  $\text{CH}_n$  resonances in methanol (below ambient) and ethylene glycol (above ambient). Standard calibration formulas included in the Varian VNMR 6.1C software were used to calculate the sample temperature. Electrospray mass spectra were measured with Sciex API III<sup>+</sup> (now Toronto, Canada) or ABI Pulsar QqT of high resolution instrument (Foster City, CA), equipped with an ion-spray source, at atmospheric pressure. UV-vis spectrometry was performed with a Hewlett-Packard/Agilent 8452A diode array spectrophotometer interfaced to an Agilent ChemStation data system (Palo Alto, CA). Preparative scale purification was performed by radial chromatography with a Harrison Research Model 7924T Chromatotron (Palo Alto, CA). Human plasma, pooled from 40 normal donors ages 16 to 65, was a gift from SomaLogic, Inc., Boulder, CO. 96-Well cell culture plates were read using a PowerWave X plate reader from BIO-TEK Instruments, Inc. (Winooski, VT), using their Kineticallc software. Flow cytometry was performed with a Becton Dickinson Biosciences FACScan (San Jose, CA) flow cytometer, using Becton Dickinson Biosciences CellQuest software. All tissue culture materials were obtained from Gibco Life Technologies (Grand Island, NY) unless otherwise noted. Cancer cells were obtained

from American Type Culture Collection (Rockville, MD), except as noted in the acknowledgments.

**2. General Procedure for the Synthesis of *p*-Nitrophenyl Carbamates of *p*-Aminobenzyl Alcohol Alkyl Carbamates.** *p*-Aminobenzyl alcohol (PABA, 1.0 mmol) was added to a dry 25 mL round-bottom flask equipped with a magnetic stir bar. Dry methylene chloride (5 mL) was added under an argon atmosphere. 4-Diisopropylethylamine (1.5 equiv) was added to the flask with stirring, followed by 1.1 equiv of the desired alkyl chloroformate by dry syringe addition. The reaction was monitored by HPLC and run until complete (typically 3 h). An additional 1.5 equiv of diisopropylethylamine was added, followed by 1.5 equiv of *p*-nitrophenyl chloroformate. The reaction was monitored by HPLC and run until complete (typically 24–48 h). After rotary evaporation, the product was purified by radial chromatography of the crude reaction mixture on a 2-mm silica gel Chromatotron plate, using a 30:1 chloroform/methanol eluent. *p*-Nitrophenyl carbamates of *p*-aminobenzyl alcohol alkyl carbamates, pure as indicated by HPLC (method 1) and <sup>1</sup>H NMR, were obtained as yellow solids in 43–65% yield over two steps.

**2.1. *p*-Nitrophenyl Carbonate of Butyl *p*-(Hydroxymethyl)phenylcarbamate.** <sup>1</sup>H NMR (CDCl<sub>3</sub>): δ 0.98 (t, 3H, *J* = 8 Hz, CH<sub>3</sub>), 1.46 (sex, 2H, *J* = 8 Hz, CH<sub>2</sub>), 1.69 (pent, 2H, *J* = 7.5 Hz, CH<sub>2</sub>), 4.21 (t, 2H, *J* = 7 Hz, OCH<sub>2</sub>), 5.27 (s, 2H, benzyl CH<sub>2</sub>), 6.89 (s, 1H, NH), 7.39–7.45 (m, 6H, benzyl and aromatic adjacent to carbonate), 8.30 (d, 2H, *J* = 10 Hz, aromatic adjacent to nitro). ESI-MS *m/z* observed, 490.6 (M + HN<sup>+</sup>Et<sub>3</sub>); calculated, 490.3 (M + HN<sup>+</sup>Et<sub>3</sub>).

**2.2. *p*-Nitrophenyl Carbonate of Pentyl *p*-(Hydroxymethyl)phenylcarbamate.** <sup>1</sup>H NMR (CDCl<sub>3</sub>): δ 0.95 (m, 3H, CH<sub>3</sub>), 1.38 (m, 4H, CH<sub>2</sub>CH<sub>2</sub>), 1.71 (m, 2H, CH<sub>2</sub>), 4.20 (t, 2H, *J* = 7 Hz, OCH<sub>2</sub>), 5.27 (s, 2H, benzyl CH<sub>2</sub>), 6.70 (s, 1H, NH), 7.39–7.42 (m, 6H, benzyl and aromatic adjacent to carbonate), 8.29 (d, 2H, *J* = 8 Hz, aromatic adjacent to nitro). ESI-MS *m/z* observed, 504.4 (M + HN<sup>+</sup>Et<sub>3</sub>); calculated, 504.3 (M + HN<sup>+</sup>Et<sub>3</sub>).

**3. General Procedure for the Synthesis of Doxazolidine Carbamates.** Either doxazolidine or doxoform, or a mixture of the two, may be used for this synthesis, but the stoichiometry must be corrected if doxoform is present because it is dimeric in doxazolidine. The syntheses of doxoform and doxazolidine were described earlier.<sup>2</sup> For the synthesis of carbamates without PABA spacer, doxazolidine (31 mg, 0.056 mmol) was added to a dry 25 mL round-bottom flask equipped with a magnetic stir bar. Dry chloroform (5 mL) was added under an argon atmosphere. 4-Dimethylaminopyridine (DMAP, 1.5 equiv, 10.2 mg) was added to the flask with stirring, followed by 0.90 equiv of the desired chloroformate by dry syringe addition. The respective *p*-nitrophenyl carbonate can be used in place of the chloroformate. With this reagent, DMAP is not used. For the synthesis of PABC-Doxaz alkyl carbamates, 1.0 equiv of the respective *p*-nitrophenyl carbonate of the *p*-aminobenzyl alkyl carbamate was added to doxazolidine in 1.0 mL of dry DMSO. The reaction was monitored by HPLC (Method 1) and run until complete (typically 2 days). After high vacuum (2 × 10<sup>-2</sup> Torr) rotary evaporation of the DMSO, the product was purified by radial chromatography of the crude reaction mixture on a 2 mm silica gel plate using a 30:1 chloroform/methanol eluent. Doxazolidine carbamates, pure as indicated by HPLC and <sup>1</sup>H NMR, were obtained as red solids in 51–83% yield, based on chloroformate or *p*-nitrophenyl carbonate as the limiting reagent.

**3.1. *N*-(Ethoxycarbonyl)doxazolidine (Doxaz Ethyl Carbamate, 1).** <sup>1</sup>H NMR (CDCl<sub>3</sub>): δ 1.30 (t, 3H, *J* = 7 Hz, β-CH<sub>3</sub>), 1.40 (d, 3H, *J* = 6 Hz, 5'-Me), 1.80 (dt, 1H, *J* = 4.5 and 16 Hz, 2'), 2.16 (dd, *J* = 4 and 15 Hz, 8), 2.1–2.4 (bm, 1H, 2'), 2.45 (bd, 1H, *J* = 14 Hz, 8), 3.03 (t, 1H, *J* = 5 Hz, 14-OH), 3.09 (dd, 1H, *J* = 1 and 19 Hz, 10), 3.33 (dd, 1H, *J* = 1 and 19 Hz, 10), 4.07 (dd, 1H, *J* = 2 and 7 Hz, 3'), 4.12 (s, 3H, 4-OCH<sub>3</sub>), 4.15 (dd, 1H, *J* = 1 and 7 Hz, 5'), 4.17 (m, 1H, 4'), 4.21 (q, 2H, *J* = 7 Hz, α-CH<sub>2</sub>), 4.79 (d, 2H, *J* = 5 Hz, 14), 4.81 (s, 1H, 9-OH), 4.9–5.1 (br m, 2H, OCH<sub>2</sub>N), 5.35 (m, 1H, 7), 5.50 (t, 1H, *J* = 6 Hz, 1'), 7.44 (d, 1H, *J* = 9 Hz, 3), 7.82 (t, 1H, *J* = 8 Hz, 2), 8.08 ppm (d, 1H, *J* =

8 Hz, 1). ESI-MS *m/z* observed, 729.2 (M + HN<sup>+</sup>Et<sub>3</sub>); calculated, 729.4 (M + HN<sup>+</sup>Et<sub>3</sub>).

**3.2. *N*-(Butyloxycarbonyl)doxazolidine (Doxaz Butyl Carbamate, 2).** <sup>1</sup>H NMR (ambient temperature, CDCl<sub>3</sub>): δ 0.91 (b, 3H, δ-CH<sub>3</sub>), 1.34 (d, 3H, *J* = 7 Hz, 5'-Me), 1.34 (b, 2H, γ-CH<sub>2</sub>), 1.60 (p, 2H, *J* = 7 Hz, β-CH<sub>2</sub>), 1.74 (bd, 1H, *J* = 15 Hz, 2'), 2.13 (dd, 1H, *J* = 4, 14 Hz, 8), 2.25 (br m, 1H, 2'), 2.42 (br d, 1H, *J* = 14 Hz, 8), 3.99 (t, 1H, *J* = 5 Hz, 14-OH), 3.01 (d, *J* = 18 Hz, 10), 3.25 (dd, 1H, *J* = 18, 2 Hz, 10), 4.04 (m, 1H, 4'), 4.07 (s, 3H, 4-OCH<sub>3</sub>), 4.09 (m, 4, 3', 5', α-CH<sub>2</sub>), 4.74 (d, 2H, *J* = 5 Hz, 14), 4.76 (s, 1H, 9-OH), 4.85–5.06 (br m, 2H, O-CH<sub>2</sub>-N), 5.30 (br s, 1H, 7), 5.45 (t, 1H, *J* = 5 Hz, 1'), 7.38 (d, 1H, *J* = 8 Hz, 3), 7.77 (t, 1H, *J* = 8 Hz, 2), 8.02 (d, 1H, *J* = 8 Hz, 1); ESI-MS *m/z* observed, 678.2175; calculated, 678.2157 (M + Na<sup>+</sup>).

**3.3. *N*-(Pentylloxycarbonyl)doxazolidine (Doxaz Pentyl Carbamate, 3).** <sup>1</sup>H NMR (ambient temperature, CDCl<sub>3</sub>): δ 0.8–0.9 (m, 3H, ε-CH<sub>3</sub>), 1.24–1.38 (m, 4H, γ-CH<sub>2</sub> and δ-CH<sub>2</sub>), 1.35 (d, 3H, *J* = 6 Hz, 5'-Me), 1.62 (bt, *J* = 7 Hz, 2H, β-CH<sub>2</sub>), 1.74 (dt, 1H, *J* = 15, 5 Hz, 2'), 2.13 (dd, 1H, *J* = 15, 5 Hz, 8), 2.2–2.3 (br m, 1H, 2'), 2.42 (br d, 1H, *J* = 15 Hz, 8), 2.99 (t, 1H, *J* = 5 Hz, 14-OH), 3.00 (d, 1H, *J* = 19 Hz, 10), 3.25 (dd, 1H, *J* = 19, 2 Hz, 10), 4.03 (m, 1H, 4'), 4.07 (s, 3H, 4-OCH<sub>3</sub>), 4.09 (m, 4H, α-CH<sub>2</sub>, 3' and 5'), 4.74 (d, 2H, 5 Hz, 14), 4.76 (s, 1H, 9-OH), 4.85–5.1 (m, 2H, O-CH<sub>2</sub>-N), 5.30 (m, 1H, 7), 5.45 (t, 1H, *J* = 5 Hz, 1'), 7.38 (d, 1H, *J* = 8 Hz, 3), 7.77 (t, 1H, *J* = 8 Hz, 2), 8.02 (d, 1H, *J* = 8 Hz, 1). ESI-MS *m/z* observed, 771.2 (M + HN<sup>+</sup>Et<sub>3</sub>); calculated, 771.4 (M + HN<sup>+</sup>Et<sub>3</sub>).

**3.4. Butyl 4-(*N*-Doxazolidinylcarbonyloxymethyl)phenylcarbamate (Butyl PABC-Doxaz, 4).** <sup>1</sup>H NMR (assignments at 55 °C from 1D proton and homonuclear COSY spectra; see Chart 2 for the numbering scheme; CDCl<sub>3</sub>) δ 0.92 (t, 3H, *J* = 7 Hz, δ-CH<sub>3</sub>), 1.33 (d, 3H, *J* = 6 Hz, 5'-Me), 1.38 (p, 2H, *J* = 7 Hz, δ-CH<sub>2</sub>), 1.61 (p, 2H, *J* = 7 Hz, β-CH<sub>2</sub>), 1.70 (dt, 1H, *J* = 15, 6 Hz, 2'), 2.12 (dd, 1H, *J* = 15, 4 Hz, 8), 2.26 (br m, 1H, 2'), 2.44 (br d, 1H, *J* = 15 Hz, 8), 2.91 (t, 1H, *J* = 5 Hz, 14-OH), 3.02 (d, 1H, *J* = 19 Hz, 10), 3.25 (dd, 1H, *J* = 19, 2 Hz, 10), 4.04 (dd, 1H, *J* = 7, 2 Hz, 4'), 4.08 (s, 3H, 4-OMe), 4.1–4.15 (m, 2H, 3' and 5'), 4.12 (t, 1H, *J* = 7 Hz, α-CH<sub>2</sub>), 4.66 (s, 1H, 9-OH), 4.72 (d, 2H, *J* = 5 Hz, 14), 4.92 (d, 1H, *J* = 4 Hz, O-CH<sub>2</sub>-N), 5.01 (b, 1H, O-CH<sub>2</sub>-N), 5.05 (b, 1H, Bn), 5.15 (b, 1H, Bn), 5.26 (br s, 1H, 7), 5.38 (t, 1H, *J* = 6 Hz, 1'), 6.84 (br s, 1H, NH), 7.29 (d, 2H, *J* = 8 Hz, PABC, 3'), 7.38 (d, 1H, *J* = 8 Hz, 3), 7.39 (d, 2H, *J* = 8 Hz, PABC 2'), 7.76 (t, 1H, *J* = 8 Hz, 2), 8.03 (d, 1H, *J* = 8 Hz, 1), 13.18 (s, 1H, phenolic-OH), 13.78 ppm (s, 1H, phenolic-OH). ESI-MS *m/z* observed, 906.8 (M + HN<sup>+</sup>Et<sub>3</sub>); calculated, 906.6 (M + HN<sup>+</sup>Et<sub>3</sub>). ESI-MS exact mass measurement with buffer-free sample showed *m/z* = 827.2616 (M + Na<sup>+</sup>); calculated, 827.2633 (M + Na<sup>+</sup>).

**3.5. Pentyl 4-(*N*-Doxazolidinylcarbonyloxymethyl)phenylcarbamate (Pentyl PABC-Doxaz, 5).** <sup>1</sup>H NMR (assignments at 55 °C from 1D proton, homonuclear COSY, HSQC, and HMBC spectra; see Chart 2 for the numbering scheme; CDCl<sub>3</sub>) δ 0.90 (t, 3H, *J* = 7 Hz, ε-CH<sub>3</sub>), 1.34 (m, 2H, γ-CH<sub>2</sub> + δ-CH<sub>2</sub>), 1.36 (d, 3H, *J* = 6 Hz, 5'-Me), 1.66 (p, 2H, *J* = 7 Hz, β-CH<sub>2</sub>), 1.72 (dt, 1H, *J* = 14, 5 Hz, 2'), 2.14 (dd, 1H, *J* = 16, 4 Hz, 8), 2.27 (br m, 1H, 2'), 2.46 (br d, 1H, *J* = 14 Hz, 8), 2.96 (t, 1H, *J* = 5 Hz, 14-OH), 3.00 (d, 1H, *J* = 18 Hz, 10), 3.24 (dd, 1H, *J* = 18, 2 Hz, 10), 4.06 (dd, 1H, *J* = 5, 2 Hz, 4'), 4.07 (s, 3H, 4-OMe), 4.09 (m, 1H, 5'), 4.13 (t, 2H, *J* = 7 Hz, α-CH<sub>2</sub>), 4.16 (m, 1H, 3'), 4.67 (s, 1H, 9-OH), 4.74 (d, 2H, *J* = 5 Hz, 14), 4.94 (d, 1H, *J* = 4 Hz, O-CH<sub>2</sub>-N), 5.03 (b, 1H, O-CH<sub>2</sub>-N), 5.06 (b, 1H, Bn), 5.16 (b, 1H, Bn), 5.26 (br s, 1H, 7), 5.40 (t, 1H, *J* = 6 Hz, 1'), 6.89 (br s, 1H, NH), 7.30 (d, 2H, *J* = 8 Hz, PABC, 3'), 7.39 (d, 1H, *J* = 8 Hz, 3), 7.41 (d, 2H, *J* = 8 Hz, PABC 2'), 7.76 (t, 1H, *J* = 8 Hz, 2), 8.02 (d, 1H, *J* = 8 Hz, 1), 13.15 (s, 1H, 11-OH), 13.78 ppm (s, 1H, 6-OH). <sup>13</sup>C NMR chemical shift assignments for protonated carbons at 55 °C from proton assignments and HSQC spectra: δ 14.1 (ε), 16.1 (5'-Me), 22.4 (δ), 28.0 (γ), 28.9 (β), 29.6 (2'), 34.2 (10), 36.0 (8), 56.9 (4-OMe), 65.6 (α), 65.6 (14), 65.9 (5'), 67.1 (Bn), 69.4 (7), 78.1 (4'), 79.5 (O-CH<sub>2</sub>-N), 100.3 (1'), 119.0 (PABC 3'), 119.0 (3), 120.1 (1), 129.5 (PABC 2'), 135.9 (2); assignment of

unprotonated carbons from the HMBC spectrum, 76.9 (9), 111.7 (10a), 112.5 (5a), 121.5 (12a), 131.6 (PABC, 1''), 133.4 (11a), 133.9 (6a), 135.8 (4a), 138.4 (PABC 4''), 153.9 (PABC CO), 157.1 (6), 161.3 (4), 187.1 (5), 187.2 (12), 213.9 ppm (13). ESI-MS  $m/z$  observed, 920.6 ( $M + \text{HN}^+\text{Et}_3$ ); calculated, 920.5 ( $M + \text{HNEt}_3$ ). ESI-MS exact mass measurement with buffer-free sample showed  $m/z = 841.2765$  ( $M + \text{Na}^+$ ); calculated, 841.2790 ( $M + \text{Na}^+$ ).

**3.6. Hydrolytic Stability.** Bovine albumin (Sigma, A-7030) was used together with DMSO to solubilize the pentyl PABC-Doxaz (5) in aqueous media at higher concentrations of prodrug. Bovine albumin (45 mg) was dissolved in 500  $\mu\text{L}$  of HPLC grade water and centrifuged at  $16\,600 \times g$  for 5 min. The upper 200  $\mu\text{L}$  was removed and used in the formulation. For the first solution, 10  $\mu\text{L}$  of 1 mM pentyl PABC-Doxaz in DMSO was mixed with 90  $\mu\text{L}$  of the bovine albumin solution, and then the mixture was diluted with 90  $\mu\text{L}$  of D-PBS. For the second solution, 10  $\mu\text{L}$  of 1 mM pentyl PABC-Doxaz in DMSO was mixed with 50  $\mu\text{L}$  of the bovine albumin solution and then diluted with 50  $\mu\text{L}$  of D-PBS and 80  $\mu\text{L}$  of fetal bovine serum. The solutions were then 53  $\mu\text{M}$  pentyl carbamate. A portion of each solution (100  $\mu\text{L}$ ) was heated at 37  $^\circ\text{C}$  for a period of 24 h, and the remainder of each solution (90  $\mu\text{L}$ ) was stored at  $-80\text{ }^\circ\text{C}$ . The heated and stored solutions were then each diluted with an equal volume of absolute ethanol to precipitate the proteins and then centrifuged at  $16\,600 \times g$  for 5 min at ambient temperature. Hydrolysis was monitored by HPLC using method 1, described under General Remarks. The chromatograms showed only pentyl PABC-Doxaz (retention time = 20 min), no hydrolysis to doxorubicin, and no loss of formaldehyde to give the corresponding pentyl PABC-Dox. The retention time of the pentyl PABC-Dox (16 min) was established with a sample formed as a byproduct of the synthesis of pentyl PABC-Doxaz and characterized by UV/vis and ESI-MS of a pure sample collected from the HPLC.

**3.7. Stability of Pentyl PABC-Doxaz in Human Plasma.** An aliquot of a 2 mM stock solution of pentyl PABC-Doxaz prodrug in DMSO was diluted with an equal volume of pharmaceutical grade Tween-80 and then further diluted to 50  $\mu\text{M}$  with pooled serum from 40 normal humans, ages 16–65 (Somalogic, Inc.). An aliquot was removed as a 0 h time point, and the remaining solution was incubated at 37  $^\circ\text{C}$  for 24 h, at which point another aliquot was removed. Proteins present in the aliquots were precipitated by dilution with an equivalent volume of absolute ethanol, followed by centrifugation at  $16\,500 \times g$  for 20 min at ambient temperature. The supernatants were analyzed by HPLC, method 2, and the reaction progress was observed by absorbance at 480 nm and fluorescence at 550 nm. The reaction was performed in triplicate. HPLC analysis indicated that, after 24 h,  $85 \pm 8\%$  of pentyl PABC-Doxaz remained intact, monitoring fluorescence at 550 nm and  $79 \pm 8\%$ , monitoring absorption at 480 nm with constant volume injection. No identifiable hydrolysis products were observed in the chromatograms.

**4. Cell Experiments.** The carcinoma cell lines SK-HEP-1, Hep G2 (HCC), MCF-7, MCF-7/Adr (breast carcinoma), DU-145 (prostate carcinoma), and SHP-77 (small cell lung carcinoma) were cultured in RPMI 1640 media containing 10% (v/v) fetal calf serum and 1% (v/v) penicillin–streptomycin (100 $\times$  solution from Gibco). The noncancerous cell lines H9c2(2-1) (rat cardiomyocytes) and Vero (green monkey kidney) were maintained in Dulbecco's modified Eagle media, supplemented with 10% (v/v) fetal calf serum and 1% (v/v) penicillin–streptomycin. All cells were grown in a humidified incubator at 37  $^\circ\text{C}$  under an atmosphere of 5%  $\text{CO}_2$  and 95% air.

**4.1. IC<sub>50</sub> Measurements.** Drug concentration in stock solutions was established by optical density at 480 nm, assuming a molar absorptivity of  $11\,500\text{ cm}^{-1}\text{M}^{-1}$  for the Dox chromophore. The cells were seeded into 96-well plates at 1000 cells/well (500 cells/well for H9c2(2-1) cells) and allowed to adhere overnight. The media was then replaced with serum-free media, containing various concentrations of Doxaz carbamate or Dox and placed into the incubator. Initially, the cells were incubated with the drugs for 3 h. Following treatment, the media was replaced with complete, fresh

media, and the cells were grown until the no-drug control lanes reached  $\sim 80\%$  confluence (3–5 days). Cells were quantified by measuring cellular metabolism of MTT, as indicated by optical density at 554 nm or by uptake of crystal violet after fixing with glutaraldehyde. Uptake of crystal violet was measured by optical density at 588 nm after solubilizing the dye in 70% ethanol. The MTT and crystal violet assays are described in detail in the literature.<sup>1,29–31</sup> The results for the 3 h incubation showed that the Doxaz carbamate prodrugs displayed detectable activity, but that the conversion to the active form had not occurred to a significant extent in 3 h. Therefore, the experiment was repeated as before, but with a 24 h incubation time. Every experiment was performed at least twice, and each condition of drug concentration was performed six times.

**4.2. Drug Uptake Measurements.** To test the efficiency of the cells for Doxaz carbamate uptake, both in the presence and in the absence of fetal bovine serum, SK-HEP-1 cells in log phase growth were dissociated with trypsin-EDTA, counted, suspended in media at  $6.7 \times 10^4$  cells/mL, plated into 6-well plates at 200 000 cells per well, and allowed to attach overnight. The media was then replaced with either fresh RPMI containing 10% fetal bovine serum or serum-free RPMI. Either Dox or Doxaz carbamate was added to the wells for a final concentration of 0.5  $\mu\text{M}$ , and the cells were incubated at 37  $^\circ\text{C}$  for five time points: 0.5, 1, 1.5, 2, and 3 h. The cells at each time point were trypsinized and analyzed by FACS, scanning for the presence of the doxorubicin fluorophore. The mean fluorescence values were then divided by the untreated control fluorescence values to calculate the relative fluorescence.

**4.3. Drug Release Measurements.** A total of 200 000 cells of either SK-HEP-1 or MCF-7/Adr lines were seeded into 6-well plates and allowed to adhere overnight in a humidified incubator at 37  $^\circ\text{C}$ . The media was then replaced with fresh, complete media containing 1% DMSO and 500 nM of either pentyl PABC-Doxaz or Dox. The cells were incubated at 37  $^\circ\text{C}$  in drug for 3 h, at which point the media was changed to drug- and DMSO-free media and incubated for time points of 0, 0.25, 0.5, 1, 2, or 3 h. All drug additions and media changes were timed such that the final incubation endpoints were reached simultaneously. The cells were then washed in cold PBS, trypsinized, and resuspended in 1 mL of ice-cold PBS and placed on ice. Observation of the Dox chromophore (excitation at 480 nm and fluorescent emission at 550 nm) by flow cytometry was performed as described in the drug uptake studies and compared to identical, untreated cells to establish background cellular fluorescence levels. The data for release of pentyl PABC-Doxaz were best fit to a double exponential rate law and for release of Dox to a single-exponential rate law.

**4.4. Measurement of mRNAs by RT-PCR Analysis.** To examine the mRNA expression of CES1 and CES2, RT-PCR was utilized. Cells in log growth phase were trypsinized and counted, and the mRNA was extracted from five million cells using the RNAqueous-4PCR kit (Ambion, Austin, TX). Candidate primer sequences were identified by Primer Express software (Applied Biosystems, Foster City, CA). Primers were selected for the 5', middle, and 3' regions of human or rat CES1 and CES2, and the selected primer sets had  $T_m$  values between 55 and 60  $^\circ\text{C}$ . The primer sequences given in Supporting Information were purchased from IDT, Inc. (Coralville, IA). The RT-PCR reaction was performed using the Access RT-PCR kit (Promega, Inc., Madison, WI) and analyzed by agarose gel electrophoresis and ethidium bromide staining.

**Acknowledgment.** The authors thank the U.S. Army Prostate Cancer Research Program (DAMD17-01-1-0046) and the National Cancer Institute of the NIH (CA-92107) for financial support, the National Science Foundation for help with the purchase of NMR equipment (CHE-0131003), Stephane Houel for exact mass measurements, William Wells for MCF-7/Adr cells, Dan Chan for SHP-77 cells, Andrew Kraft for DU-145 cells, Tapestry Pharmaceuticals for Tween 80, and SomaLogic for plasma.

**Supporting Information Available:** HPLC of Doxaz carbamates, monitoring at 274 and 480 nm with two different buffers; NMR spectra for Doxaz carbamates; Eyring and Arrhenius plots for the conformational change of Doxaz ethyl carbamate; and primer sequences for RT-PCR. This material is available free of charge via the Internet at <http://pubs.acs.org>.

## References

- Fenick, D. J.; Taatjes, D. J.; Koch, T. H. Doxoform and daunoform: Anthracycline-formaldehyde conjugates toxic to resistant tumor cells. *J. Med. Chem.* **1997**, *40*, 2452–2461.
- Post, G. C.; Barthel, B. L.; Burkhart, D. J.; Hagadorn, J. R.; Koch, T. H. Doxazolidine, a proposed active metabolite of doxorubicin that cross-links DNA. *J. Med. Chem.* **2005**, *48*, 7648–7657.
- Cutts, S. M.; Nudelman, A.; Rephaeli, A.; Phillips, D. R. The power and potential of doxorubicin–DNA adducts. *IUBMB Life* **2005**, *5*, 73–81.
- Minotti, G.; Menna, P.; Salvatorelli, E.; Cairo, G.; Gianni, L. Anthracyclines: Molecular advances and pharmacologic developments in antitumor activity and cardiotoxicity. *Pharmacol. Rev.* **2004**, *56*, 185–229.
- Shimma, N.; Umeda, I.; Arasaki, M.; Murasaki, C.; Masubuchi, K.; et al. The design and synthesis of a new tumor-selective fluoropyrimidine carbamate, Capecitabine. *Bioorg. Med. Chem.* **2000**, *8*, 1697–1706.
- Walko, C. M.; Lindley, C. Capecitabine: A review. *Clin. Ther.* **2005**, *27*, 23–44.
- Quinney, S. K.; Sanghani, S. P.; Davis, W. I.; Hurley, T. D.; Sun, Z. M. D. J.; et al. Hydrolysis of Capecitabine to 5'-deoxy-5-fluorocytidine by human carboxylesterases and inhibition by loperamide. *J. Pharmacol. Exp. Therap.* **2005**, *313*, 1011–1016.
- Tabata, T.; Katoh, M.; Tokudome, S.; Nakajima, M.; Yokoi, T. Identification of the cytosolic carboxylesterase catalyzing the 5'-deoxy-5-fluorocytidine formation from capecitabine in human liver. *Drug Metab. Dispos.* **2004**, *32*, 1103–1110.
- Miwa, M.; Ura, M.; Nishida, M.; Sawada, N.; Ishikawa, T.; et al. Design of a novel oral fluoropyrimidine carbamate, Capecitabine, which generates 5-fluorouracil selectively in tumors by enzymes concentrated in human liver and cancer tissue. *Eur. J. Cancer* **1998**, *34*, 1274–1281.
- Xu, G.; Zhang, W.; Ma, M. K.; McLeod, H. L. Human carboxylesterase 2 is commonly expressed in tumor tissue and is correlated with activation of irinotecan. *Clin. Cancer Res.* **2002**, *8*, 2605–2611.
- Sanghani, S. P.; Quinney, S. K.; Fredenburg, T. B.; Sun, Z. M. D. J.; Davis, W. I.; et al. Carboxylesterases expressed in human colon tumor tissue and their role in CPT-11 hydrolysis. *Clin. Cancer Res.* **2003**, *9*, 4983–4991.
- Bencharit, S.; Morton, C. L.; Yu, X.; Potter, P. M.; Redinbo, M. R. Structural basis of heroin and cocaine metabolism by a promiscuous human drug-processing enzyme. *Nat. Struct. Biol.* **2003**, *10*, 349–356.
- Bencharit, S.; Morton, C. L.; Howard-Williams, E. L.; Danks, M. K.; Potter, P. M.; et al. Structural insights into CPT-11 activation by mammalian carboxylesterases. *Nat. Struct. Biol.* **2002**, *9*, 337–342.
- Bencharit, S.; Morton, C. L.; Hyatt, J. L.; Kuhn, P.; Danks, M. K.; et al. Crystal structure of human carboxylesterase 1 complexed with the Alzheimer's drug Tacrine: From binding promiscuity to selective inhibition. *Chem. Biol.* **2003**, *10*, 341–349.
- Martin, M. L.; Mabon, F.; Trierweller, M. The problem of rotational entropy contributions in carbamates and thiocarbamates. NMR multicoalescence and saturation transfer experiments. *J. Phys. Chem.* **1981**, *85*, 76–78.
- Gunther, H. *NMR Spectroscopy*, 2nd ed.; John Wiley: New York, NY, 1992; pp 361–363.
- de Groot, F. M. H.; de Bart, A. C. W.; Verheijen, J. H.; Scheeren, H. W. Synthesis and biological evaluation of novel prodrugs of anthracyclines for selective activation by the tumor-associated protease plasmin. *J. Med. Chem.* **1999**, *42*, 5277–5283.
- Dinaut, A. N.; Taylor, S. D. Antibody-catalyzed activation of a model tripartate prodrug by tandem hydrolysis–1,6-elimination reaction. *Chem. Commun.* **2001**, 1386–1387.
- de Graaf, M.; Nevalainen, T. J.; Scheeren, H. W.; Pinedo, H. M.; Haisma, H. J.; et al. A methylester of the glucuronide prodrug DOX-GA3 for improvement of tumor-selective chemotherapy. *Biochem. Pharmacol.* **2004**, *68*, 2273–2281.
- Carl, P. L.; Chakravarty, P. K.; Katzenellenbogen, J. A. A novel connector linkage applicable in prodrug design. *J. Med. Chem.* **1981**, *24*, 479–480.
- Lampidis, T. J.; Kolonias, D.; Podona, T.; Isreal, M.; Safa, A. R.; et al. Circumvention of P-GP MDR as a function of anthracycline lipophilicity and charge. *Biochemistry* **1997**, *36*, 2679–2685.
- Rooseboom, M.; Commandeur, J. N. M.; Vermeulen, N. P. E. Enzyme-catalyzed activation of anticancer prodrugs. *Pharmacol. Rev.* **2004**, *56*, 53–102.
- Hennenfent, K. L.; Govindan, R. Novel formulations of taxanes: A review. Old wine in a new bottle? *Ann. Oncol.* **2006**, *17*, 735–749.
- London, W. T. Hepatocellular carcinoma: etiology and pathogenesis. *ASCO Educational Book*; 34th Annual Meeting of the American Society of Clinical Oncology, 1998; p 168.
- Keller, J. W.; Peacock, J. L. Cancer of the major digestive glands: pancreas, liver, bile ducts, gallbladder. *Clinical Oncology, A Multidisciplinary Approach for Physicians and Students*; 7th ed.; W.B. Saunders: Philadelphia, PA, 1993; p 597.
- Blum, H. E. Hepatocellular carcinoma: Therapy and prevention. *World J. Gastroenterol.* **2005**, *11*, 7391–7400.
- Thomas, M. B.; Abbruzzese, J. L. Opportunities for targeted therapies in hepatocellular carcinoma. *J. Clin. Oncol.* **2005**, *23*, 8093–8108.
- Mizokami, M.; Tanaka, Y. Molecular evolutionary analysis predicts the incidence of hepatocellular carcinoma in the United States and Japan. *Cancer Chemother. Pharmacol.* **2004**, *54* (Suppl 1), S83–S86.
- Mosmann, T. Rapid colorimetric assay for cellular growth and survival: Application to proliferation and cytotoxicity assays. *J. Immunol. Methods* **1983**, *65*, 55–63.
- Gilles, R. J.; Didier, N.; Denton, M. Determination of cell number in monolayer cultures. *Anal. Biochem.* **1986**, *159*, 109–113.
- Reile, H.; Birnböck, F.; Bernhardt, G. T.; Spruss, H. S. Computerized determination of growth kinetic curves and doubling times from cells in microcultures. *Anal. Biochem.* **1990**, *187*, 262–267.

JM060597E